Water Science & Technology

IWA PUBLISHING

Water Science & Technology Vol 87 No 7, 1672 doi: 10.2166/wst.2023.083

Removal of phosphate with a polyacrylonitrile composite functionalized by a metal organic framework-enhanced layered double hydroxide

Jianzhi Song[a], Ligen Cha[b], Mika Sillanpää[c,d,e,f] and Tuomo Sainio[g,*]

[a] School of Engineering Science, LUT University, Sammonkatu 12, Mikkeli 50130, Finland
[b] Department of Chemical and Metallurgical Engineering, School of Chemical Engineering, Aalto University, Kemistintie 1, Espoo, P.O. Box 16100, FI-00076, Finland
[c] Department of Chemical Engineering, School of Mining, Metallurgy and Chemical Engineering, University of Johannesburg, P.O. Box 17011, Doornfontein 2028, South Africa
[d] Department of Applied Physics, Faculty of Science and Technology, Universiti Kebangsaan Malaysia, Bangi, Selangor 43600, Malaysia
[e] Zhejiang Rongsheng Environmental Protection Paper Co. Ltd, No. 588 East Zhennan Road, Pinghu Economic Development Zone, Zhejiang 314213, China
[f] International Research Centre of Nanotechnology for Himalayan Sustainability (IRCNHS), Shoolini University, Solan, Himachal Pradesh 173212, India
[g] School of Engineering Science, LUT University, Mukkulankatu 19, Lahti 15210, Finland
*Corresponding author. E-mail: tuomo.sainio@lut.fi

TS, 0000-0002-4951-8711

ABSTRACT

Excessive phosphorus causes eutrophication problems. The adsorptive removal of phosphate is prevalent and practical in large-scale applications, such as column adsorption. A metal organic framework (MOF)-enhanced layered double hydroxide (LDH) adsorbent material was developed and studied for batch adsorption and then combined with polyacrylonitrile (PAN) to form MOF/LDH/PAN composite beads working as a functional material for columns. Scanning electron microscopy (SEM) images showed the well-dispersed adsorbent powder in porous composite beads. The Fowler–Guggenheim isotherm model described the phosphate adsorption behavior of the MOF/LDH powder with a maximum capacity of 74.96 mg P/g. Mass transfer in the composite beads was successfully described with the Fickian diffusion model. The composite-packed fixed bed treated 37.95 BVs of the influent (55.51 mg P/L phosphate solution) and achieved an uptake of 18.92 mg P/g, with a removal efficiency of 96.42%, before the breakthrough point in the column study. The phosphate-loaded composite bed was regenerated with 0.1 M NaOH to 70% efficiency within 30 BVs. The polymer composite can be considered a practical solution for adsorption-based water treatment applications in tank and column processes where powder adsorbents cannot be applied.

Key words: column adsorption, layered double hydroxide, metal organic framework, phosphate adsorption, polyacrylonitrile polymer composite

HIGHLIGHTS

- Zn- and Al-based LDH were enhanced with MOF to produce a new adsorbent material for phosphate removal.
- The synthesized adsorbent outperformed both precursors regarding phosphate adsorption.
- The Fowler–Guggenheim isotherm suggests repulsive interactions between adsorbates.
- Polyacrylonitrile-supported MOF/LDH/PAN composite beads perform well in an adsorption column.

GRAPHICAL ABSTRACT

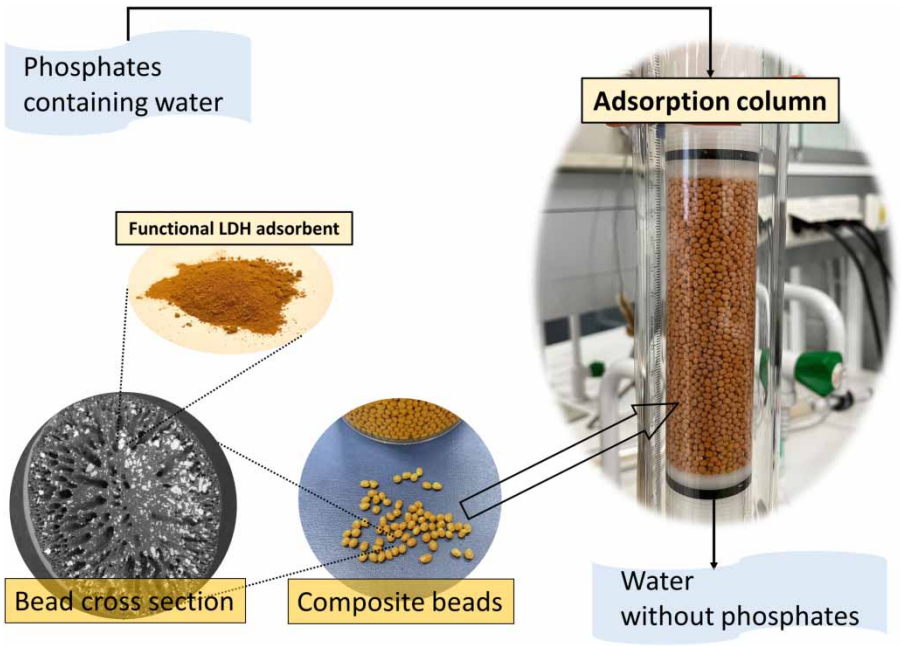

1. INTRODUCTION

Phosphorus (P) is an essential mineral element for many different organisms, but it causes eutrophication problems when present in excessive amounts in surface water bodies. Further degradation of water quality and the death of aquatic life follow the unrestrained algal bloom and aquatic plant growth caused by excessive enrichment with minerals and nutrients, particularly P and nitrogen. P, mainly in the form of phosphate, enters natural water bodies through agricultural runoff, sewage discharge, and industrial wastewater, such as from slaughterhouses (Bunce *et al.* 2018). Thus, phosphates are regarded as pollutants whose concentrations need to be diminished by water treatment.

Technologies for phosphate removal include biological wastewater treatment processes using microorganisms or algae-based systems, chemical precipitation (e.g., struvite), and physicochemical methods such as adsorption, ion exchange, and membrane filtration. The most common treatment option for phosphate removal is chemical precipitation, which is reliable and controllable but requires the addition of large-quantity chemicals and the post-treatment of sludge (Cheng *et al.* 2009). The adsorption technique is also prevalent because it can treat waste streams with low concentrations at high efficiency and is relatively inexpensive and environmentally friendly (sludge-free) (Shraddha *et al.* 2018).

Numerous adsorbents have been studied and employed for phosphate treatment, such as zeolites, silica materials, metal oxides and hydroxides, clay minerals, activated carbon and biochar, and polymers (Bacelo *et al.* 2020). The use of layered double hydroxides (LDHs) for anion adsorption has received increasing attention in recent years due to their anion exchangeability. LDHs consist of metal ions, hydroxyl groups, and certain intercalated anions with a common formula of $[M^{3+}_{x}M^{2+}_{1-x}(OH)_2]A^{n-}_{x/n}{\cdot}yH_2O$, where M^{3+} and M^{2+} represent the metal cations, A^{n-} is the anion, and x is located in the range of 0.18 – 0.33 (Iftekhar *et al.* 2018). LDHs have been studied as adsorbents for the treatment of phosphates in wastewater, either in their pristine form or after being modified and combined with other compounds (Mandel *et al.* 2013; Yan *et al.* 2018). At the same time, another emerging functional material, the metal organic framework (MOF), has been developed as an advanced solid adsorbent for phosphate treatment. Researchers have applied MOFs based on iron (Nehra *et al.* 2019), zirconium (Lin *et al.* 2015), zeolitic imidazolate frameworks (ZIFs) (Shams *et al.* 2016), and many other compounds for the adsorption of phosphates. Additionally, designs of MOF/layered double hydroxide (LDH) composites, whether MOF derived from LDH or vice versa, have been utilized for separation purposes. A partially converted LDH-ZIF-8 membrane has also been used for gas separation (Liu *et al.* 2015) and Mg–Al-LDH-supported Cu-MOF has been

fabricated for the removal of methyl orange dye (Chakraborty & Acharya 2018). Based on findings from MOF/LDH studies, the combination of LDH and MOF might have great promise for adsorption applications.

To the best of our knowledge, few reported studies have investigated the adsorption of phosphate by MOF/LDH composite materials. The hypothesis that MOF/LDH composite is effective for the adsorption of phosphates led to the present study, which investigated MOF/LDH integration and phosphate adsorption. Furthermore, the usability of the adsorbent in practical applications was considered because the particle sizes of the aforementioned MOF/LDH materials were determined to lie between 0.2 and 1 μm (Liu *et al.* 2015; Chakraborty & Acharya 2018). Such small particles lead to an extremely high-pressure drop in columns and carryover in stirred tanks, which makes their use not feasible. To ensure the usability of the adsorbent in practical applications, a polymer-based composite was prepared using polyacrylonitrile (PAN) as a binding polymer with an as-synthesized adsorbent powder. PAN was selected for its porous character and durability, which make it suitable to function as a carrier of the adsorbent powder. Moreover, the form of the polymer composite is favorable for large-scale adsorption processes. The composite has low-pressure drop and is stable at typical application temperatures (15–35 °C). Further, PAN is known to be chemically stable and has good mechanical durability. The gelation of the PAN-based composite (MOF/LDH/PAN) is accomplished in water after heating at a mild temperature, which demands less chemical and energy input (Xu *et al.* 2018).

2. MATERIALS AND EXPERIMENTAL METHODS

2.1. Materials

The chemicals utilized in the present study were obtained from Sigma-Aldrich and used without further purification. The chemicals that were used included sodium hydroxide (NaOH), hydrochloric acid (HCl), nitric acid (HNO_3), trimesic acid (benzene-1,3,5-tricarboxylic acid, $C_6H_3(CO_2H)_3$, H_3BTC), ferrous chloride tetrahydrate ($FeCl_2{\cdot}4H_2O$), dimethylformamide (DMF), methanol (CH_3OH), aluminum nitrate nonahydrate ($Al(NO_3)_3{\cdot}9H_2O$), zinc nitrate hexahydrate ($Zn(NO_3)_2{\cdot}6H_2O$), Tween 80, PAN (150,000 MW, $(C_3H_3N)_n$), and monopotassium phosphate (KH_2PO_4).

2.2. Synthesis

2.2.1. Synthesis of the MOF MIL-100(Fe)

The synthesis procedure of MIL-100(Fe) was adapted from Guesh *et al.* (2017) with modifications (Guesh *et al.* 2017). First, 1.676 g H_3BTC was dissolved in a 22.8 mL NaOH (1 M) solution (Solution 1) and 2.26 g ferrous chloride tetrahydrate was dissolved in 97.2 mL water (Solution 2). Solution 1 was then added dropwise into Solution 2 while stirring. The mixture was stirred for 24 h at room temperature. Centrifugation was applied to separate the solid from the liquid. The collected solid was further purified using DMF and methanol successively for 24 h. The washed compound was then dried overnight in a vacuum oven at 80 °C.

2.2.2. Synthesis of the MOF/LDH

The as-synthesized MIL-100(Fe) (500 mg) was mixed with aqueous solutions of 0.5 M $Al(NO_3)_3{\cdot}9H_2O$ (8.5 mL) and 1 M $Zn(NO_3)_2{\cdot}6H_2O$ (8.5 mL). The mixture was then sonicated for 30 min. NaOH (1 M) solution was dripped into the mixture until the pH became 10. The resultant substance was aged overnight at 60 °C while undergoing magnetic stirring (about 18 h). The product was then centrifuged and washed thoroughly with water. Finally, the product was freeze-dried for 48 h.

2.2.3. Synthesis of the MOF/LDH/PAN composite

The method for the synthesis of MOF/LDH/PAN composite was adapted from previously published studies (Xu *et al.* 2018) and amended according to the needs of the present study. First, 3.6 g MOF/LDH was mixed with 42 mL DMF and 1 mL Tween 80 by stirring at 60 °C for 2 h. Then, 2.4 g PAN powder was gradually added. Heating and stirring continued for another 2 h. The mixture was pumped into deionized water through a 0.7 mm needle while being stirred. The gelled composites were then left to age in water for 24 h. Finally, the composites were rinsed with more than 2 L warm water. The synthesized products were then stored hydrated in water without drying.

2.3. Characterization

Various techniques were utilized for the characterization of the as-synthesized products, MOF/LDH powder, and MOF/LDH/PAN composite. Phase identification was done via X-ray diffraction (XRD, PANalytical X-ray diffractometer) with Co Kα irradiation at $\lambda = 1.79$ Å, and 2θ of 5°–80°. Surface functional groups were identified by Fourier transform infrared

spectroscopy (FTIR, Bruker Vertex 70 model) in a spectra range of 4,000−400 cm^{-1}. The morphology was imaged using scanning electron microscopy (SEM). The applied SEM devices were the JEOL JSM-7900F and Hitachi SU3500. A cross-section sample of the composite was prepared via razor blade cutting in a liquid nitrogen environment. Transmission electron microscopy (TEM) was conducted using a Hitachi HT-7700. The specific surface area and pore size distribution were determined via N_2 adsorption–desorption isotherm analysis (Tristar® II Plus). The particle size of the MOF/LDH powder was investigated with a Malvern Zetasizer (Nano ZEN350).

The MOF/LDH/PAN composite was tested for moisture and ash contents. It was centrifuged at 3,000 rpm for 10 min to remove the excess water content. The moisture content was measured based on centrifuged composite samples dried overnight at 105 °C. For ash content determination, the standard test method for ash content in plastics, ASTM D5630-01, was used. The composite dimensions were analyzed using a Raman imaging microscope (Thermo Scientific DXR3xi). The chemical stability against acidic solutions was investigated by immersing the composite samples in HNO_3 solutions with various pH levels (1, 1.5, 2, 2.5, and 3) and shaking them mildly (50 rpm) for 5 days at room temperature. The weight losses of the samples were then recorded.

2.4. Batch adsorption and desorption

Batch adsorption equilibrium experiments were performed for the MIL-100(Fe), LDH, MOF/LDH powder, and MOF/LDH/PAN composite. The adsorption of phosphate on the inert PAN polymer was not studied. Sorption kinetics was studied with MOF/LDH and MOF/LDH/PAN to see the effect of the matrix and particle size on the diffusion rates. The synthetic solution (KH_2PO_4) used for adsorption was controlled to have a background ionic strength (I) of 20 mM through the addition of 1 M NaCl solution. The batch studies were conducted at 15, 25, and 35 °C for 48 h, with intermediate handshaking and four-time pH adjustments to maintain a uniform mild acidic condition (pH 5.9−6.1) during the adsorption process. The kinetic studies were conducted in a 500 mL KH_2PO_4 solution with intense motor mixing at 800 rpm at 25 °C, with pH adjustment and small-volume sampling at pre-defined time intervals.

Desorption tests were performed for the MOF/LDH powder in batch experiments with NaOH solutions of various concentrations (0.1–2 M). The whole process was accomplished without drying or changing the container. Adsorption was first done in a 200 mL stock solution (approximately 50 mg P/L) for 0.1 g MOF/LDH powder for 24 h with mild rotation. The solid and liquid were then separated through centrifugation, decanting, and washing with water. NaOH solutions were added to regenerate the adsorbent and the volume of the regeneration solution was adjusted to 20 mL. Samples were collected after 24 h rotation. The desorption rate was calculated by dividing the mass of the desorbed P by the mass of the adsorbed P. The percentages of the released Zn, Al, and Fe were based on the mass of the adsorbent.

The concentrations of the tested solutions and samples were examined via inductively coupled plasma optical emission spectrometry (ICP-OES, Thermo iCAP 6300 series). Thus, all the concentrations in the present study are shown herein as the mass of P.

All the batch tests were conducted in triplicate. Each data point was plotted separately in figures instead of applying error bars because there is experimental uncertainty also in the equilibrium liquid phase concentration values. It improved the accuracy, especially in the nonlinear fitting of the isotherm plots and gave a better understanding of the quality of the data.

2.5. Column adsorption using the composite

The as-synthesized MOF/LDH/PAN composite was used as the filling material in the column process to study its performance in phosphate recovery. The column had an inner diameter of 2.5 cm and was filled with the composite to pack a 10 cm bed. Thus, the bed volume (BV) was 49.09 cm^3 , where BV refers to the volume of the inner-column space packed with the adsorbent bed. The whole process was conducted at room temperature (in this case, 25 °C). In the loading step, the influent solution (approximately 50 mg P/L) was fed into the column with the downward flow at a flow rate of 2 BV/h (1.636 mL/min) for 100 BVs. Effluent samples were taken for each BV. The regeneration was started immediately after the loading step; 0.1 M NaOH was used as the desorbing agent, with the upward flow at a flow rate of 5 BV/h (4.091 mL/min) for 30 BVs. One sample was taken every two bed volumes. The samples were then analyzed with ICP-OES.

3. RESULTS AND DISCUSSION

3.1. Characterization of the functional material and MOF/LDH/polyacrylonitrile composite

The structures of the as-synthesized powdery materials (MIL-100(Fe), LDH, and MOF/LDH) were compared using XRD and FTIR. The MOF/LDH material is a compound based on the LDH structure, which is revealed by the similarity between the identical peaks in the XRD patterns of the LDH and MOF/LDH, as shown in Figure 1(a). The peaks located at 10° and 20° in the MOF/LDH pattern indicate MIL-100(Fe) crystals (Xie *et al.* 2017). A more detailed XRD pattern of the LDH is shown in Figure S1 in the supplementary material. The FTIR spectrum of the MOF/LDH shows the bands of both the MIL-100(Fe) and LDH. The broad band at around 3,400 cm^{-1} in the MOF/LDH spectrum corresponds to the same area in the LDH, which is assigned to hydroxyl group (−OH) stretching vibration. The carboxylic groups in the MIL-100(Fe) and the bending hydroxyl groups contribute to the bands at around 1,600 cm^{-1}. The strong band at 1,384 cm^{-1} in the MOF/LDH spectrum was attributed to the nitrogen–oxygen bonds of nitrate (He *et al.* 2010). The bands between wavenumbers 800 and 400 cm^{-1} represent the metal–oxygen bonds in the LDH and the carbon–hydrogen bonds of benzene in the MIL-100(Fe) (Iftekhar *et al.* 2018; Nehra *et al.* 2019). Both bands appeared in the MOF/LDH spectrum, indicating the co-existence of LDH and MIL-100(Fe). The detailed FTIR spectra of the MIL-100(Fe), LDH, and MOF/LDH are shown in Figures S2–4.

The N_2 adsorption–desorption isotherm of the MOF/LDH was shown as Type IV with an H3 hysteresis loop, as can be seen in Figure S5. The pore size was 9.28 nm according to the pore size analysis using the Barrett, Joyner, and Halenda (BJH) method. As the BJH method underestimates the pore size by 20–30% for narrow mesopores with a $< \sim 10$ nm diameter, the amended pore size was 11.6−13.3 nm (Thommes *et al.* 2015). The BET-specific surface area of the MOF/LDH was 136 m^2/g. It is improved by 42.45% compared to that of the LDH, which was 95.47 m^2/g. Obviously, this is due to the

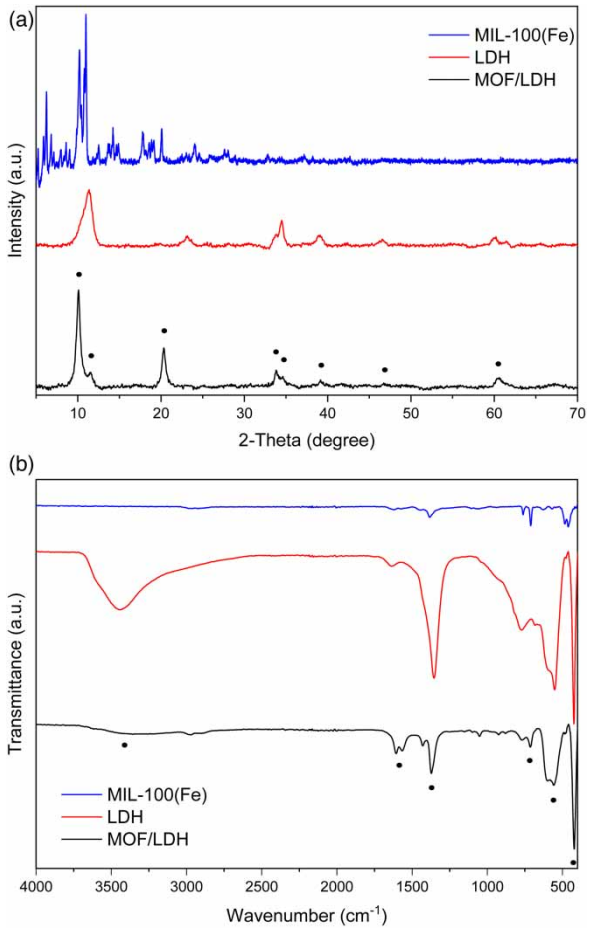

Figure 1 | (a) XRD patterns and (b) Fourier transform infrared spectroscopy spectra of the MOF, LDH, and MOF/LDH composite materials.

high specific surface area of the MIL-100(Fe) content of the MOF/LDH. The average diameter of the MOF/LDH particle samples was 0.566 μm.

The SEM images of the MOF/LDH powder (Figure 2(a)) and MOF/LDH/PAN composite (Figure 2(b) and 2(c)) showed the morphologies of the powdery and polymer composite products. In the presence of the MIL-100(Fe), the MOF/LDH retained the layered structure, while particles dispersed all over. The active material was not evenly distributed inside the composite shell. The active material tended to gather in certain sections of the composite, probably due to the impact of gravity when the raw mixture was extruded from the syringe to form a drop and the centrifugal forces during the gelation of the composite. More sophisticated processes, such as the use of double nozzles with pressurized air, may be able to prevent uneven distribution. The cross-section of the MOF/LDH/PAN composite showed a highly porous structure at both the macroscale (~0.1 mm) and microscale (~1 μm). The porous structure eases the mass transfer of the liquid and the intraparticle diffusion provides support for better adsorption, which is a favorable characteristic for an adsorbent material. TEM images of MIL-100(Fe) and MOF/LDH are shown in Figure S6. The MIL-100(Fe) structure was presented accompanying the layers of LDH in the image of MOF/LDH, which confirmed the combination of the materials.

The moisture content of the swollen composite sample was 77.60% (wet weight basis). The ash contents of the MOF/LDH powder and the MOF/LDH/PAN composite were 72.02 and 34.06% (dry weight basis), respectively. Thus, the dry weight-based MOF/LDH content of the MOF/LDH/PAN composite was 47.29% and the wet weight-based MOF/LDH content was 10.59%.

The composite samples were presented as ellipsoidal spheres. The ellipsoidal form was due to the dropping of the homogeneous mixed liquid into the gelation medium and the stretching because of stirring. A total of 111 composite samples were analyzed via Raman microscopy, some of which are shown in Figure 3. The circularity of the projection areas of the composites was 0.89 and the average length and width axes were 2,710 and 2,050 μm, respectively.

The mass losses of the composite samples treated with HNO_3 solutions in the durability test are shown in Table 1. At a pH of below 2, the composite lost 4.59–6.35% of its total mass. The mass loss was negligible at pH 2.5 and no mass loss was found at pH 3, showing that the composite is acid resistant and stable above pH 2.

3.2. Adsorption isotherms and kinetics

Three adsorption isotherms based on different assumptions about molecular-level interactions were included in this study: the Langmuir, Freundlich, and the Fowler–Guggenheim isotherms. The Langmuir isotherm (Equation (1)) assumes monolayer adsorption on a homogeneous adsorbent:

$$q_e = \frac{q_m K_L C_e}{1 + K_L C_e} \tag{1}$$

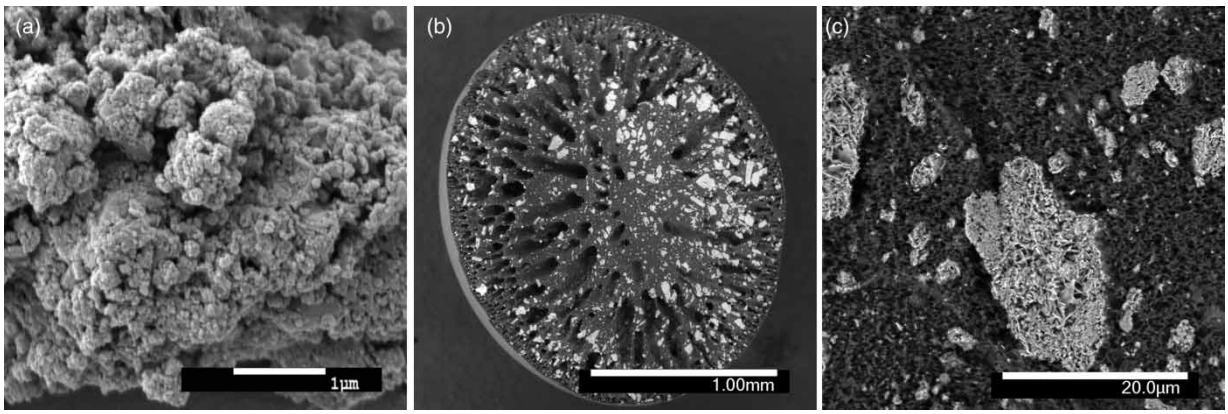

Figure 2 | SEM images of (a) MOF/LDH powder; (b) MOF/LDH/PAN composite cross-sections; and (c) one spot of the MOF/LDH/PAN composite cross-sections.

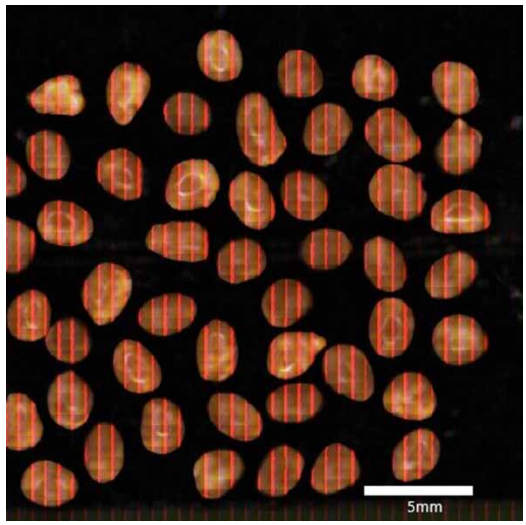

Figure 3 | Example of the Raman image of the MOF/LDH/PAN composite samples for the determination of the particle dimensions.

Table 1 | Stability of the MOF/LDH/PAN composite in HNO_3 solutions at 25 °C for 5 days

pH	1	1.5	2	2.5	3
Mass loss (%)	6.35	5.19	4.59	0.59	0.00

where C_e (mg/L) is the equilibrium concentration of phosphorus; q_e (mg/g) and q_m (mg/g) are the equilibrium and maximum uptake capacities of phosphorus, respectively; and K_L (L/mg) is the Langmuir constant.

The Freundlich isotherm (Equation (2)) assumes multilayer adsorption onto heterogeneous surfaces:

$$q_e = K_f C_e^{\frac{1}{n}} \tag{2}$$

where n is the heterogeneity factor related to the distribution of the interaction energies of the adsorption sites and K_f (mg/g·(L/mg)$^{1/n}$) represents the Freundlich constant.

The Fowler–Guggenheim isotherm (Equation (3)) assumes the same homogeneous adsorbent surface as the Langmuir isotherm but also considers the interactions between the adsorbed species:

$$K_{FG} C_e = \frac{q_e}{q_m - q_e} \exp\left(-\chi \frac{q_e}{q_m}\right) \tag{3}$$

where χ reflects the lateral interactions between the adsorbates and K_{FG} represents the Fowler–Guggenheim constant.

All the models were fitted to the measured loadings using nonlinear regression. Linearization of the models and the data was avoided because such manipulation affects the weights of the data points and the residuals. The parameters obtained with the three isotherm models are listed in Table 2 and the isotherm plots are shown in Figure 4.

The Freundlich model predicts an infinite uptake capacity for further C_e and results in an infinite slope (dq/dC) toward extremely diluted conditions. Thus, the Freundlich model cannot be considered a preferred model to explain the adsorption process, although it seems to fit the measured data well. The maximum Langmuir adsorption capacity was found to be 60.86 mg P/g. However, the Langmuir isotherm model is not suitable for the isotherm data of the MOF/LDH in this study because, as can be seen in Figure 4, it underestimates the uptake capacity at a higher concentration range.

Fitting of the Fowler–Guggenheim model gave a higher R^2 than for the Langmuir isotherm. It should be noted that there are three parameters in the Fowler–Guggenheim model but only two parameters in the Langmuir isotherm. The improvement

Table 2 | Parameters of the nonlinear fitted isotherm models of MOF/LDH powder at 25 °C

Isotherm	Parameter			R^2
Langmuir	q_m (mg P/g)	K_L (L/mg)		0.9293
	60.86	6.10		
Freundlich	N	K_f (mg/g·(L/mg)$^{1/n}$)		0.9679
	7.67	45.20		
Fowler–Guggenheim	q_m (mg P/g)	K_{FG} (L/g)	χ	0.9993
	74.96	35.71	−5.38	

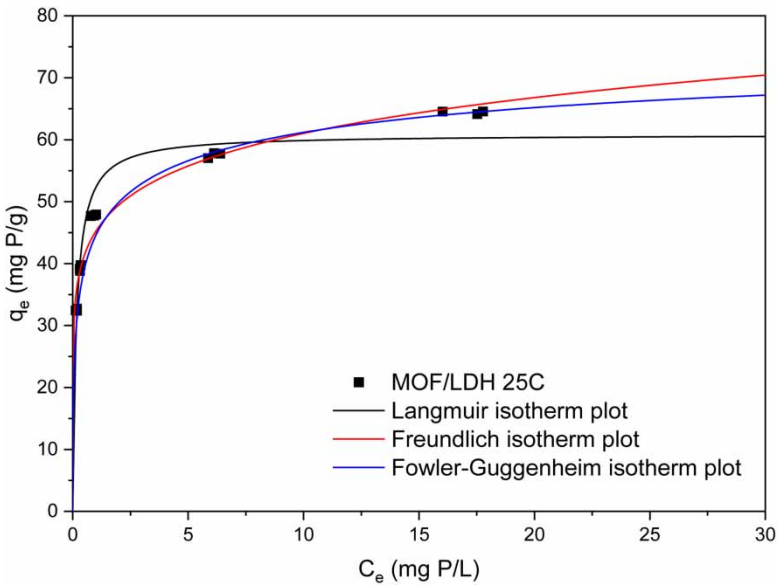

Figure 4 | Nonlinear fitted isotherm plots of MOF/LDH powder at 25 °C (batch adsorption experiments, C_0 ~50 mg P/L KH_2PO_4 solution, 48 h equilibrium with intermediate handshaking, and pH adjusted to 5.9−6.1, four times).

in fit – both quantitatively (R^2) and qualitatively (the shape of the calculated isotherm) – is so significant that introducing an additional adjustable parameter is justified. The Langmuir isotherm levels off too early, whereas the Fowler–Guggenheim isotherm correctly predicts monotonically increasing adsorption. It is therefore concluded that the interaction between adsorbate molecules is not a negligible factor. The negative value of χ (−5.38) indicated repulsive interactions between the adsorbed phosphate ions. The maximum adsorption capacity was 74.96 mg P/g.

To illustrate the comparison of the adsorption capacity between the developed adsorbent and the precursors, the batch adsorption data of the MOF/LDH, MIL-100(Fe), and LDH at 25 °C are shown in Figure 5(a). As can be clearly seen in Figure 5(a), the uptake capacity of the as-synthesized adsorbent MOF/LDH was promoted by the LDH–MIL-100(Fe) combination. The MOF/LDH outperformed both precursors as an adsorbent for phosphate. The adsorption behaviors of the MOF/LDH powder and MOF/LDH/PAN composite at different temperatures are shown in Figure 5(b). The differences between the adsorption isotherms at various temperatures for both samples are insufficiently clear to analyze. This effect is attributed to the better accessibility of the adsorption sites due to a more flexible structure at high temperatures. On the other hand, a low temperature is more desirable for adsorption reactions that release heat. Thus, the temperature effect was not shown as a regular trend. The adsorption capacity (unit mass) of the MOF/LDH/PAN composite is approximately one-tenth that of the MOF/LDH because of the mass of the polymer structure. However, the polymer composite is in a form that favors adsorption process operations, such as an adsorption column. A column can be designed to pack a large

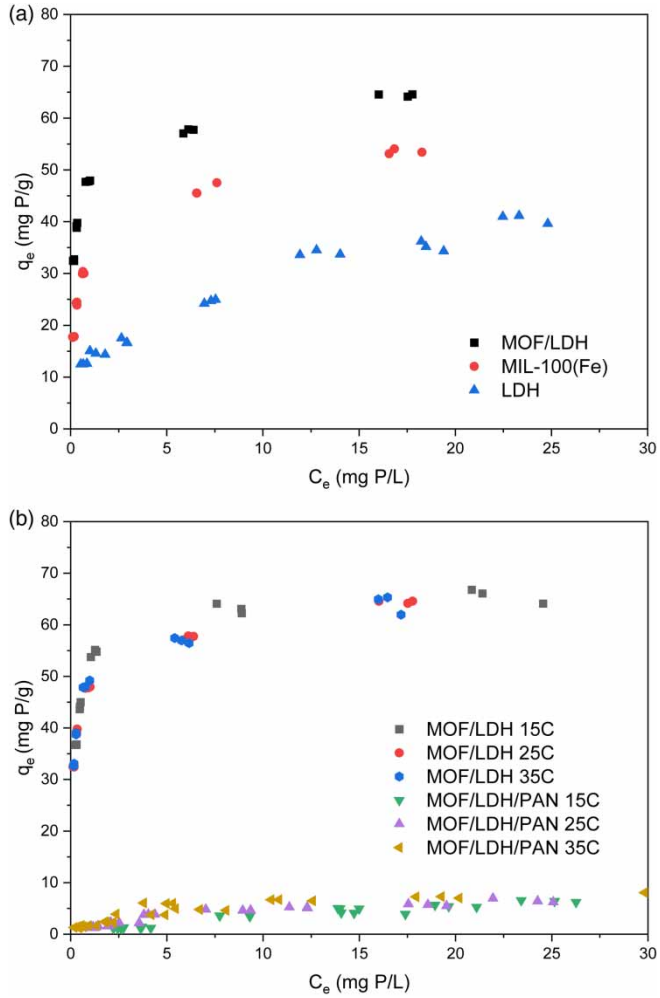

Figure 5 | (a) Adsorption equilibrium data of MOF/LDH, MOF, and LDH at 25 °C; (b) MOF/LDH powder and MOF/LDH/PAN composite at 15, 25, and 35 °C (batch adsorption experiments, C_0 ~50 mg P/L KH_2PO_4 solution, 48 h equilibrium with intermediate handshaking, and pH adjusted to 5.9−6.1, four times).

volume of the polymer composite to achieve a high capacity. However, this approach is not applicable with MOF/LDH in powder form.

Kinetic studies were carried out on the MOF/LDH powder and the MOF/LDH/PAN composite. As observed in Figure 6, the uptake rate was initially very high with the powder. The phosphate concentration in the liquid phase dropped from 70 to 44mg P/L in 1 min. In contrast, with the PAN composite beads, the same change in liquid phase concentration took 90 min.

The kinetic data were correlated with an intraparticle diffusion model. The PAN particles were assumed to be spherical, with a diameter equal to the Sauter diameter determined for the somewhat elliptic PAN particles. The powder particles were assumed to be spherical, with a diameter equal to the measured mean diameter. The diffusive flux of phosphate was calculated using Fick's law, which leads to the following differential mass balance equation:

$$\frac{\partial q_P}{\partial t} = \frac{1}{r^2}\frac{\partial}{\partial r}\left(r^2 D_{s,P}\frac{\partial q_P}{\partial r}\right) \tag{4}$$

where q_P is the local loading of P (mg/m^3), r is the radial coordinate (m), and $D_{s,P}$ is the diffusion coefficient of phosphate (m^2/s). The spatial derivatives were calculated with five-point centered finite-difference approximations in the interior points and biased lower-degree approximations near the boundaries of the spatial domain. The surface of the particle was

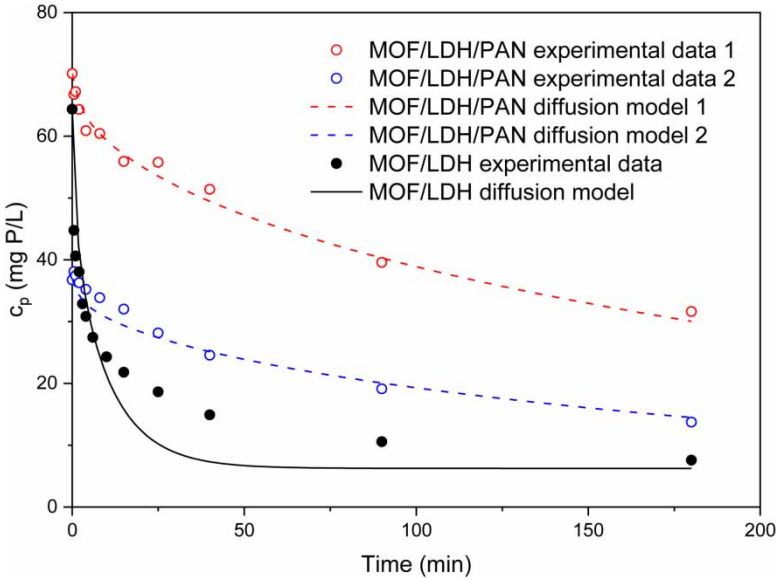

Figure 6 | Kinetics of phosphate uptake in the MOF/LDH powder (filled circles, solid line) and in the MOF/LDH/PAN composite (open circles, dashed lines). Batch experiments at 25 °C, 500 mL KH_2PO_4 solution, motor mixing at 800 rpm, pH: 5.9−6.1, powder mass: 500 mg, and composite mass: 3,750 mg.

assumed to be constantly at equilibrium with the bulk liquid phase. In other words, q_P ($r = R_p$) was calculated using the Fowler–Guggenheim equation, with the parameters given in Table 2. The condition of no flux through the center of the particle was applied as another boundary condition.

The rate of concentration change in the liquid phase was derived from the constraint of no accumulation of mass at the surface of the particle, which led to:

$$\frac{\partial c_P}{\partial t} = -\left(D_{s,P}\frac{\partial q_P}{\partial r}\bigg|_{r=R_p}\right)\frac{3}{R_p}\frac{m_{ads}}{\rho_{ads}}\frac{1}{V^L} \tag{5}$$

Equations (4) and (5) were integrated numerically with initial conditions $c_P = c_{0,P}$ and $q_P(r) = 0$ using a variable step: the use of a variable-order integrator (`ode15s` in Matlab). The diffusion coefficients of phosphate in the powder and composite beads and the mass fraction of LDH-MOF in the beads were estimated using a simplex-type direct search algorithm (`fminsearch` in Matlab).

The reasonably good agreement of the Fickian diffusion model with the PAN composite experiment data indicates that intraparticle diffusion is the rate-limiting factor in the adsorption process of the composite (Figure 6). A 2.21×10^{-12} m^2/s diffusion coefficient is in the range typical for porous adsorbents. However, in the case of the powder, the intraparticle diffusion model failed to explain the measured data. The best-fit value for the diffusion coefficient is 7.88×10^{-18} m^2/s, which is unreasonably small and cannot be regarded as physically meaningful. The most plausible explanation for this is that the small particles ($R_p = 0.28 \times 10^{-6}$ m) have moved with the liquid in the stirred tank. This results in a low slip velocity at the phase boundary and, thus, high liquid film mass transfer resistance.

While the kinetics of phosphate sorption into the powder material (MOF/LDH) is higher than in the MOF/LDH/PAN composite, the foreseeable high-pressure drop in columns and carryover in stirred tanks make the use of the powder in large-scale applications not feasible. On the other hand, the polymer composite (MOF/LDH/PAN) containing functional adsorbent can be packed in a column for a large volume to achieve a high column capacity.

3.3. Desorption of phosphate

The desorption of phosphate from the MOF/LDH powder was done using NaOH aqueous solutions with various concentrations in batch experiments. The results are shown in Table 3. The release of Fe was negligible, which indicates that the MOF component of the composite is stable at least until 1.0 mol/L of NaOH. Release of Al and Zn was not significant until 0.2 mol/L of NaOH, indicating that the LDH component was stable at low NaOH concentrations. Although the desorption rate of P reached 71.30% with 0.5 M NaOH, the severe Zn release at and above 0.5 mol/L NaOH was a decisive factor in rejecting the use of high concentrations of NaOH. The desorption rate of P under 0.1 NaOH had a minimal difference from that under 0.2 M NaOH. To retain the adsorbent material and ensure that it would have good stability in cyclic separation, 0.1 M NaOH was chosen as the regeneration media in the later column tests.

3.4. Adsorption and regeneration of phosphate in the column

In this study, the breakthrough point was defined as the bed volumes fed to the column when the cumulative effluent concentration reached 2 mg P/L, which was decided according to European Union regulations concerning treated wastewater quality (Preisner *et al.* 2020). The breakthrough curve is shown in Figure 7(a). It is a flat profile corresponding to inefficient mass transfer due to the large size of the composite beads.

The cumulative concentration of P in the effluent reached 1.99 mg P/L at the breakthrough point of 38.0 BVs. More detailed data are shown in Figures S7–9. At the breakthrough point, the uptake of P in the fixed bed was 18.92 mg P/g, and the removal efficiency from the fed 1.86 L phosphate solution with a 55.51 mg P/L concentration was 96.42%. As adsorption on the MOF/LDH/PAN composite is clearly mass transfer limited, even better performance is expected when the synthesis procedure is modified to produce smaller particles.

As shown in Table 4, the column adsorption performance of the current composite is very good compared to that of the other materials used in previous studies. The studies listed in Table 4 have shown large differences in feed concentration, flow rates, and not all their data are directly comparable. The higher the feed concentration, the earlier the bed is saturated and the earlier the breakthrough is expected to occur. Similarly, the higher the flow rate (in units of BV/h), the higher the mass transfer resistance and the earlier the breakthrough.

The Al_2O_3/calcium alginate composite material (Ai *et al.* 2022) was studied with a flow rate and particle size comparable to those in the present study. The amount of P removed per unit mass of adsorbent at breakthrough point was eight times larger with the MOF/LDH/PAN composite than with the Al_2O_3/calcium alginate. In another study with a comparable particle size (Jung *et al.* 2017), modified biochar calcium alginate beads were able to purify 25 BV of feed when the feed concentration was approximately one-third that in the present study. The flow rate, however, was higher than in the present study.

Among the materials that have been studied for application in the column adsorption of phosphate (Wu *et al.* 2007; Woumfo *et al.* 2015; Jung *et al.* 2017; Ramirez *et al.* 2018; Ye *et al.* 2019; Ai *et al.* 2022), the MOF/LDH/PAN composite in the present study possesses the highest total P uptake capacity (36.93 mg P/g).

The regeneration efficiency of the adsorbent determines the usability of the composite for practical applications. In the present study, desorption was conducted with the chosen desorbing agent, 0.1 M NaOH. As shown in Figure 7(b), the desorbing agent led to an asymmetrical desorption curve for the effluent P concentrations. In the beginning, the sharp peak that formed followed by a long-tail decline demonstrated that much of the desorption occurred during the first 6 BVs of regeneration. About 60% regeneration efficiency had already been reached with a 9.7 BV desorbing agent, but 70% efficiency consumed a 27.2 BV desorbing agent (Figure S10). Nuryadin and Imai reported the column regeneration of phosphate-saturated

Table 3 | Phosphate desorption from MOF/LDH powder

NaOH (M)	Desorption rate of P (%)	Released Zn (%)	Released Al (%)	Released Fe (%)
0.1	40.11	0.22	0.81	0.00
0.2	45.05	1.39	1.22	0.00
0.5	71.30	24.29	4.76	0.00
1.0	67.88	26.74	5.25	0.00
2.0	60.79	26.35	5.28	0.01

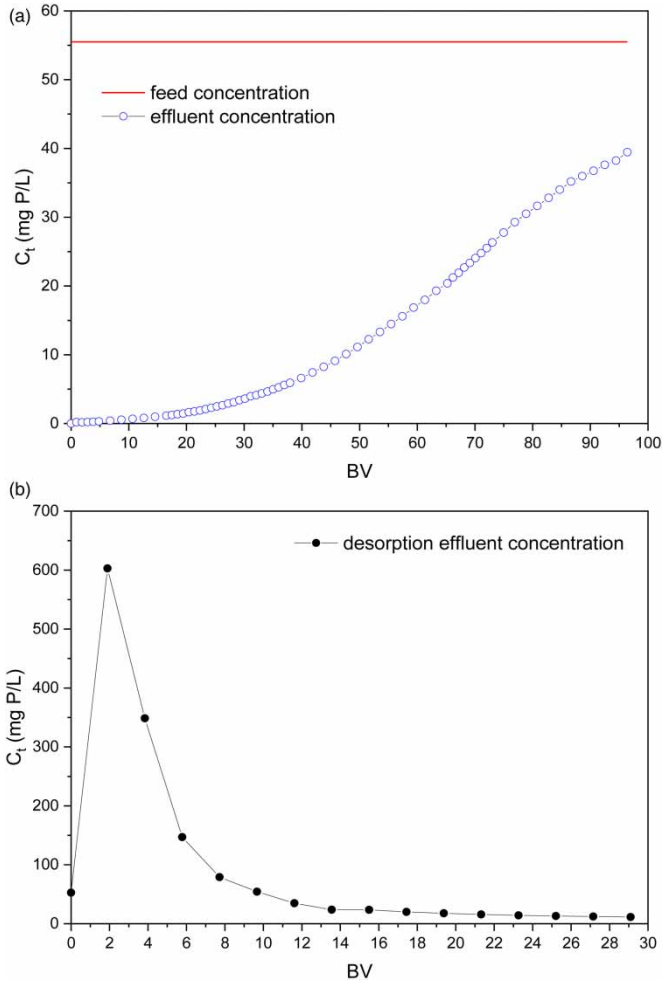

Figure 7 | Column (a) adsorption and (b) desorption data curves (temperature 25 °C, column diameter 2.5 cm, bed height 10 cm, BV 49.09 mL, bed material MOF/LDH/PAN composite; loading with downward flow, flow rate: 2 BV/h, influent KH_2PO_4 solution C_0: 55.51 mg P/L; regenerating with upward flow, flow rate: 5 BV/h, and desorbing agent: 0.1 M NaOH).

amorphous Zr/MgFe-LDH composite with 0.1 N NaOH as a desorbing agent, in which 91.70% desorption efficiency was achieved with 127.1 BV of desorbing agent, and 98.80% was finally achieved with 1,016.9 BV (8 h operation) (Nuryadin & Imai 2021).

Overall, the MOF/LDH/PAN composite is a usable and promising material in the column adsorption process of phosphate.

4. CONCLUSION

In the present study, an LDH-based adsorbent material was synthesized with an MIL-100(Fe) as a precursor. The MIL-100(Fe)-enhanced MOF/LDH adsorbent powder was then combined with PAN to form MOF/LDH/PAN composite beads working as a functional material. The composite, which is in the form of a polymer bead, is a favorable adsorbent form to use in adsorption processes such as adsorption columns. XRD and FTIR confirmed MIL-100(Fe) loading in the adsorbent material. SEM images clearly showed the porous structure of the composite beads and the well-dispersed adsorbent powder inside the composite. The phosphate adsorption behavior of the MOF/LDH powder was reasonably well described by the Fowler–Guggenheim isotherm model. The kinetic behavior of the composite was described by the Fickian intraparticle diffusion model. The diffusion coefficients are in the range typical for polymeric adsorbents, but a large particle size leads to high mass transfer resistance. The uptake capacity of the powder adsorbent reached 74.96 mg P/g, while the composite had a

Table 4 | Adsorption of phosphate in columns packed with various separation materials (masses of phosphate are given as elemental phosphorus)

Adsorbent			Fixed bed dimension			Column operation			Column performance		
	D_p (mm)	m_{ads} (g)	d (cm)	h (cm)	BV (mL)	C_0 (mg P/L)	Q (mL/min)	Q (BV/h)	V_b (BVs)	q_b (mg P/g)	q_e (mg P/g)
MOF/LDH/PAN composite (this study)	2.38	5.28	2.5	10	49.09	55.51	1.636	2	38.0	18.92	36.93
Al_2O_3/calcium alginate composite (Ai *et al.* (2022))	~3.25	6	2	12.5	39.25	4.97	3	4.59	71.1	2.27	7.08
Modified biochar calcium alginate bead (Jung *et al.* (2017))	1.85		1	15	11.78	13.04	5	25.48	25.3		1.89
HFeO dispersed within anion exchange resin (IRA-400) (Ramirez *et al.* (2018))	~0.49	1.22	1.1	2	1.9	100	1	31.58	87.9		34.64
La(III)-chelex-100 resin (Wu *et al.* (2007))	0.3–0.15	2	1	2.55	2	154.85	3	90	10.0		3.04
Andosol-bagasse 50/50 mixture (Woumfo *et al.* (2015))	≤0.16	1	3.1	1.8	13.58	3.26	4	17.67	17.7		1.36
MgOP composite (Ye *et al.* (2019))	0.074	4	4	5.2	65.31	6.52	16	14.7	9.6		3.12

D_p, particle size (diameter) of adsorbent; m_{ads}, adsorbent mass; d, column inner diameter; h, bed height; BV, bed volume; C_0, feed concentration; P, phosphorus; Q, flow rate; V_b, breakthrough point; q_b, uptake of P at breakthrough point; q_e, uptake of P at equilibrium; MOF/LDH/PAN, metal organic framework/layered double hydroxide/polyacrylonitrile; MgOP, magnesia-pullulan composite.

good phosphate removal ability but adsorbed less per unit mass due to the polymer structure. Nevertheless, the polymer composite form can be considered a practical solution for adsorption-based water treatment applications in tank and column processes. The composite-packed fixed bed (49.09 mL) treated 38.0 BVs (1.86 L) of the influent solution with 55.51 mg P/L phosphate. An 18.92 mg P/g uptake with 96.42% removal efficiency before the breakthrough point was achieved in the column adsorption study. The phosphate-loaded composite bed was regenerated with 0.1 M NaOH up to 70% efficiency within 30 BVs.

Overall, the MOF/LDH/PAN composite is potentially applicable to remove and/or recover phosphates in large-scale column adsorption processes where powder materials cannot be used due to high-pressure drops. However, the particle size of the composite must be reduced and the weight fraction of the active material (now 10–20%) must be increased by modifying the synthesis process. In addition, further studies should focus on simplifying the complicated synthesis procedures, reducing the use of, and increasing the percentage of the reuse of DMF and Tween 80, which would lead to a greener and more sustainable route.

ACKNOWLEDGEMENT

This work was supported by European Regional Development Fund project ID A73961.

DATA AVAILABILITY STATEMENT

All relevant data are included in the paper or its Supplementary Information.

CONFLICT OF INTEREST

The authors declare there is no conflict.

REFERENCES

Ai, H., Xu, L., Zhang, Z., Hu, X., Chen, C., Sun, W., Fu, M.-L. & Yuan, B. 2022 Al_2O_3 encapsulated by calcium alginate as composite for efficient removal of phosphate from aqueous solutions: batch and column studies. *Water Science and Technology* **85** (11), 3315–3330. doi:10.2166/wst.2022.173.

Bacelo, H., Pintor, A. M. A., Santos, S. C. R., Boaventura, R. A. R. & Botelho, C. M. S. 2020 Performance and prospects of different adsorbents for phosphorus uptake and recovery from water. *Chemical Engineering Journal* **381**, 122566. doi:10.1016/J.CEJ.2019.122566.

Bunce, J. T., Ndam, E., Ofiteru, I. D., Moore, A. & Graham, D. W. 2018 A review of phosphorus removal technologies and their applicability to small-scale domestic wastewater treatment systems. *Frontiers in Environmental Science* **6** (FEB), 8.

Chakraborty, A. & Acharya, H. 2018 Facile synthesis of MgAl-layered double hydroxide supported metal organic framework nanocomposite for adsorptive removal of methyl orange dye. *Colloids and Interface Science Communications* **24** (March), 35–39. doi:10.1016/j.colcom.2018.03.005.

Cheng, X., Huang, X., Wang, X., Zhao, B., Chen, A. & Sun, D. 2009 Phosphate adsorption from sewage sludge filtrate using zinc–aluminum layered double hydroxides. *Journal of Hazardous Materials* **169** (1–3), 958–964. doi:10.1016/J.JHAZMAT.2009.04.052.

Guesh, K., Caiuby, C. A. D., Mayoral, Á., Díaz-García, M., Díaz, I. & Sanchez-Sanchez, M. 2017 Sustainable preparation of MIL-100(Fe) and its photocatalytic behavior in the degradation of methyl orange in water. *Crystal Growth & Design* **17** (4), 1806–1813. doi:10.1021/acs.cgd.6b01776.

He, H., Kang, H., Ma, S., Bai, Y. & Yang, X. 2010 High adsorption selectivity of ZnAl layered double hydroxides and the calcined materials toward phosphate. *Journal of Colloid and Interface Science* **343** (1), 225–231. doi:10.1016/j.jcis.2009.11.004.

Iftekhar, S., Küçük, M. E., Srivastava, V., Repo, E. & Sillanpää, M. 2018 Application of zinc-aluminium layered double hydroxides for adsorptive removal of phosphate and sulfate: equilibrium, kinetic and thermodynamic. *Chemosphere* **209**, 470–479. doi:10.1016/J.CHEMOSPHERE.2018.06.115.

Jung, K. W., Jeong, T. U., Choi, J. W., Ahn, K. H. & Lee, S. H. 2017 Adsorption of phosphate from aqueous solution using electrochemically modified biochar calcium-alginate beads: batch and fixed-bed column performance. *Bioresource Technology* **244**, 23–32. doi:10.1016/j.biortech.2017.07.133.

Lin, K. Y. A., Chen, S. Y. & Jochems, A. P. 2015 Zirconium-based metal organic frameworks: highly selective adsorbents for removal of phosphate from water and urine. *Materials Chemistry and Physics* **160**, 168–176. doi:10.1016/j.matchemphys.2015.04.021.

Liu, Y., Peng, Y., Wang, N., Li, Y., Pan, J. H., Yang, W. & Caro, J. 2015 Significantly enhanced separation using ZIF-8 membranes by partial conversion of calcined layered double hydroxide precursors. *ChemSusChem* **8** (21), 3582–3586. doi:10.1002/cssc.201500977.

Mandel, K., Drenkova-Tuhtan, A., Hutter, F., Gellermann, C., Steinmetz, H. & Sextl, G. 2013 Layered double hydroxide ion exchangers on superparamagnetic microparticles for recovery of phosphate from waste water. *Journal of Materials Chemistry A* **1** (5), 1840–1848. doi:10.1039/C2TA00571A.

Nehra, M., Dilbaghi, N., Singhal, N. K., Hassan, A. A., Kim, K. H. & Kumar, S. 2019 Metal organic frameworks MIL-100(Fe) as an efficient adsorptive material for phosphate management. *Environmental Research* **169**, 229–236. doi:10.1016/J.ENVRES.2018.11.013.

Nuryadin, A. & Imai, T. 2021 Application of amorphous zirconium (hydr)oxide/MgFe layered double hydroxides composite in fixed-bed column for phosphate removal from water. *Global Journal of Environmental Science and Management* **7** (4), 485–502. doi:10.22034/gjesm.2021.04.01.

Preisner, M., Neverova-Dziopak, E. & Kowalewski, Z. 2020 An analytical review of different approaches to wastewater discharge standards with particular emphasis on nutrients. *Environmental Management* **66** (4), 694–708. doi:10.1007/s00267-020-01344-y.

Ramirez, A., Giraldo, S., García-Nunez, J., Flórez, E. & Acelas, N. 2018 Phosphate removal from water using a hybrid material in a fixed-bed column. *Journal of Water Process Engineering* **26**, 131–137. doi:10.1016/J.JWPE.2018.10.008.

Shams, M., Dehghani, M. H., Nabizadeh, R., Mesdaghinia, A., Alimohammadi, M. & Najafpoor, A. A. 2016 Adsorption of phosphorus from aqueous solution by cubic zeolitic imidazolate framework-8: modeling, mechanical agitation versus sonication. *Journal of Molecular Liquids* **224**, 151–157. doi:10.1016/j.molliq.2016.09.059.

Shraddha, K., Dipika, J. & Arti, M. 2018 Green and eco-friendly materials for the removal of phosphorus from wastewater. *Life Cycle Assessment of Wastewater Treatment* 199–219. doi:10.1201/9781315165820-10.

Thommes, M., Kaneko, K., Neimark, A. V., Olivier, J. P., Rodriguez-Reinoso, F., Rouquerol, J. & Sing, K. S. W. 2015 Physisorption of gases, with special reference to the evaluation of surface area and pore size distribution (IUPAC technical report). *Pure and Applied Chemistry* **87** (9–10), 1051–1069. doi:10.1515/pac-2014-1117.

Woumfo, E. D., Siéwé, J. M. & Njopwouo, D. 2015 A fixed-bed column for phosphate removal from aqueous solutions using an andosol-bagasse mixture. *Journal of Environmental Management* **151**, 450–460. doi:10.1016/j.jenvman.2014.11.029.

Wu, R. S. S., Lam, K. H., Lee, J. M. N. & Lau, T. C. 2007 Removal of phosphate from water by a highly selective La(III)-Chelex resin. *Chemosphere* **69** (2), 289–294. doi:10.1016/j.chemosphere.2007.04.022.

Xie, Q., Li, Y., Lv, Z., Zhou, H., Yang, X., Chen, J. & Guo, H. 2017 Effective adsorption and removal of phosphate from aqueous solutions and eutrophic water by Fe-based MOFs of MIL-101. *Scientific Reports* **7** (1), 1–15. doi:10.1038/s41598-017-03526-x.

Xu, J., Virolainen, S., Zhang, W., Kuva, J., Sainio, T. & Koivula, R. 2018 Polyacrylonitrile-encapsulated amorphous zirconium phosphate composite adsorbent for Co, Nd and Dy separations. *Chemical Engineering Journal* **351**, 832–840. doi:10.1016/J.CEJ.2018.06.112.

Yan, H., Chen, Q., Liu, J., Feng, Y. & Shih, K. 2018 Phosphorus recovery through adsorption by layered double hydroxide nano-composites and transfer into a struvite-like fertilizer. *Water Research* **145**, 721–730. doi:10.1016/J.WATRES.2018.09.005.

Ye, Y., Jiao, J., Kang, D., Jiang, W., Kang, J., Ngo, H. H., Guo, W. & Liu, Y. 2019 The adsorption of phosphate using a magnesia–pullulan composite: kinetics, equilibrium, and column tests. *Environmental Science and Pollution Research* **26** (13), 13299–13310. doi:10.1007/s11356-019-04858-z.

First received 4 November 2022; accepted in revised form 9 March 2023. Available online 21 March 2023